Journal of Nanobiotechnology

RESEARCH

Open Access

Small extracellular vesicle-based one-step high-throughput microfluidic platform for epithelial ovarian cancer diagnosis

Yu Wu[1,4,5,6†], Chao Wang[2†], Yuhan Guo[1,4,5,6†], Yunhong Zhang[2], Xue Zhang[2], Pan Wang[1,4,5,6], Wei Yue[1,4,5,6], Xin Zhu[1,4,5,6], Zhaofei Liu[7], Yu Zhang[2,3*], Hongyan Guo[1,4,5,6*], Lin Han[2,3*] and Mo Li[1,4,5,6*]

Abstract

Background Ovarian cancer (OC) is diagnosed at advanced stages, resulting in limited treatment options for patients. While early detection of OC has been investigated, the invasiveness of approaches, high sample requirements, or false-positive rates undermined its benefits. Here, we present a "one-step" high-throughput microfluidic platform for epithelial ovarian cancer (EOC) detection that integrates small extracellular vesicle (sEV) capture, in situ lysis, and protein biomarker detection.

Results We identified 1,818 differentially expressed proteins (DEPs) through proteomic analysis of sEVs from patients' serum, combined with cell lines. Through multi-step screening of DEPs, we identified EOC biomarkers to customize the microfluidic platform. We used the microfluidic platform to test the expression of EOC biomarkers with 2 μL of serum from 209 participants in a prospective cohort. Based on the test results, an EOC detection model (P9) was constructed, which achieved a sensitivity of 92.3% (95% CI, 75.9–97.9%) for stage I, 90.0% (95% CI, 69.9–97.2%) for stage II at a specificity of 98.8% (95% CI, 93.6–99.8%) in the training set. The specificities reached 98.8% (95% CI, 93.6–99.8%) in the training set and 100.0% (95% CI, 91.6–100.0%) in the validation set of a held-out group of 105 participants. A model combining the P9 and patient's CA125 value exhibited 100.0% (95% CI, 95.6–100%) specificity in both training and validation, without compromising sensitivity.

Conclusions We developed a non-invasive high-throughput microfluidic platform for EOC sEV-derived biomarker detection. It significantly reduced false positives and sample volume. Given its convenience and low cost, this platform could advance OC early detection to benefit of women.

†Yu Wu, Chao Wang and Yuhan Guo contributed equally to this work.

*Correspondence:
Yu Zhang
yuzhang@sdu.edu.cn
Hongyan Guo
bysyghy@163.com
Lin Han
hanlin@sdu.edu.cn
Mo Li
limo@hsc.pku.edu.cn

Full list of author information is available at the end of the article

Keywords Microfluid platform, Small extracellular vesicles (sEVs), Proteome, Epithelial ovarian cancer (EOC), Cancer early diagnosis

Background

Ovarian cancer (OC) is the leading gynecologic malignancy responsible for high mortality rates, mainly due to its covert symptoms and consequently delayed diagnosis. Around 90% of OC cases are epithelial ovarian cancer (EOC), one of the most aggressive malignant neoplasms [1], whose 5-year survival rate drops from 92% at the early stage to 29% at the late stage [2–4]. Despite advancements in cancer detection, the early diagnosis of EOC remains remarkably challenging. Hitherto, two multicenter clinical trials for OC screening were accomplished using transvaginal ultrasonography (TVS) and CA125 [5, 6]. Intriguingly, a further study revealed that the serial changes of CA125 or the Risk of Ovarian Cancer Algorithm (ROCA), outperformed CA125 with a fixed cutoff in the same cohort [7, 8], highlighting the significance of biomarker selection for the EOC screening. Using the ROCA, the United Kingdom Collaborative Trial of Ovarian Cancer Screening (UKCTOCS), the largest randomized clinical trial assessing the effect of screening on an average-risk population, exhibited a significant stage shift toward early stages [5], rendering more patients the opportunity for curative treatments. It is notable that, due to the reported harms of invasive examination for TVS and overtreatment for considerable false-positive results, those conventional modalities are not recommended as standard of care. Hence, approaches that minimize invasiveness and false positives are key to benefiting EOC patients from cancer early detection.

Small extracellular vesicles (sEVs) are present in the body fluids of all organisms, carrying primarily proteins and other substrates. sEVs derived from tumors contain pathological information and biomolecules that reflect the real-time state of living cancer cells, providing a relatively complete picture of cancer progression at all stages. This makes sEVs an attractive approach for early cancer detection [9–11]. sEV-based cancer early detection has been studied in lung cancer, hepatocellular carcinoma, pancreatic ductal adenocarcinoma, and others [12–16]. However, the enrichment and purification of sEVs from limited clinical samples, such as blood or urine, hinder the effective detection of sEV-derived biomarkers. Hence, more attention has been attracted to modalities for sEVs enrichment and purification, such as size-exclusion filtration, immunoaffinity, and acoustic-fluid-based technologies, to overcome clinical limitations [17, 18]. Although some methods aimed to detect cancerous biomarkers from isolated sEVs [19–23], these approaches have primarily targeted surface proteins, thereby overlooking the potential of the enriched proteins within sEVs derived from living cancer cells. Therefore, there is a need for a device that can effectively enrich sEVs from limited clinical samples and detect targeted biomarkers in real-world scenarios.

Herein, we developed a rapid, cost-effective microfluidic platform for early EOC detection, achieving "one-step" sEV cargo detection by integrating sEV capture, in situ lysis, and protein biomarker detection. Through proteomic analysis of sEVs from EOC patient serum and tumor cell lines, we identified 1,818 differentially expressed proteins (DEPs) compared to healthy controls. After functional analysis and antibody evaluation, 12 elevated proteins were selected as biomarker candidates linked to pathways such as Ras signaling and tumor metastasis. These biomarkers were used to construct the detection platform, which quantified serum biomarkers in 125 patients. A model built on 9 biomarkers achieved a specificity of 98.8% (95% CI, 93.6–99.8%) in the training set and 100.0% (95% CI, 91.6–100.0%) in validation, with further improvements when combined with CA125. This study demonstrates a versatile platform for sEV-based biomarker detection, offering a practical tool for EOC early diagnosis and broader biomarker discovery.

Materials and methods

Sample collection

Between March 2021 and February 2024, we enrolled consecutive OC patients who underwent radical surgery in the Department of Obstetrics and Gynecology of Peking University Third Hospital. A total of 200 patients with EOC and 136 healthy controls were prospectively enrolled, and 10 mL of blood samples were obtained during pre-radical resection surgery. The demographic and clinical information of all participants in this study including age, CA125, International Federation of Gynecology and Obstetrics (FIGO) stage, grade, and histological subtypes was recorded in Table S1.

The inclusion and exclusion criteria were stated as follows. In brief, patients with OC who provided written consent and met the following criteria were enrolled: (1) aged between 18 and 75 years and (2) OC was newly clinically diagnosed by computed tomography and pathologically confirmed EOC. The exclusion criteria were as follows: (1) participants who received an organ transplant, prior non-autologous bone marrow transplant, or stem cell transplant, (2) participants who were diagnosed with other malignancies, (3) participants who had an immune disorder or autoimmune disease, (4) participants received any anti-cancer treatment 30 days

before the expected enrollment date due to any non-cancer diseases, (5) participants who receive blood transfusion within 30 days before expected enrollment date, and (6) pregnant or lactating participants. For healthy individuals, the inclusion criteria were (1) provided written consent, (2) aged between 18 and 75 years, and (3) no malignant diseases. The above exclusion criteria also applied to healthy individuals, and those who were suspected to have any type of OC were excluded.

All human materials used in this study were approved by the Medical Science Research Ethics Committee of Peking University Third Hospital (IRB00006761-M2019291). All participants voluntarily signed a declaration of informed consent.

Preparation of sEV-capture microfluidic chips and sEV-detection microarray chips

To produce graphene oxide quantum dots (GOQDs)-assembled glass substrate, glass slides (CITOTEST, China, P/N. 80302-0001) were sequentially subjected to ultrasonic cleaning in deionized water, ethanol, and deionized water for 10 min each, followed by drying with nitrogen (N_2) to maintain a clean glass surface. One side of the slides was treated with oxygen plasma for 10 min to form surface hydroxyl groups, followed by a 45-min immersion in a 3-aminopropyltriethoxysilane (APTES) solution. The slides were then ultrasonically cleaned in deionized water and dried with N_2. APTES-treated slides were immersed in a 1 mg/mL GOQD solution for 45 min, cleaned ultrasonically in deionized water, and dried with N_2. The GOQDs were immobilized on the glass surface via the reaction between their carboxyl groups and the amino groups on APTES.

Microfluidic chips were fabricated via soft lithography technology. Negative photoresist SU8-2025 (KAYAKU, Japan, Y111069) was used for photolithography to create the silicon-based mold for the chip. The PDMS prepolymer and curing agent (Corning, USA, Sylgard 184) were mixed at a 10:1 ratio, poured into the mold, and cured in a drying oven at 80 °C for 1 h. The GOQDs-assembled glass substrate was bonded to the antibody barcode chip, and the target antibody was introduced to form an antibody barcode array on the glass substrate. The antibody barcode glass substrate was combined with the microarray PDMS chip to form an antibody-barcode microarray chip. Each sample loading well covers a whole antibody array. The sEV-capture chip was obtained by bonding a through-hole PDMS chip and a GOQDs-assembled glass substrate, with the bottom substrate in the through-hole fixed with sEV-capture antibodies. For sEV capture, 4 μL of 100 μg/mL CD63 antibody (Sigma, Cat#CBL553) was added to each microwell and incubated overnight under a sealing film. Removal of incubation solution and followed by blocking with 3% BSA for 10 min and sequential washing with 1 × PBS and distilled water to remove unbound components. For sEV enrichment, 2 μL of serum sample was added to each well and incubated for 60 min, then removed supernatant and washed with 1 × PBS. The captured sEVs were lysed in situ by adding 5 μL of radio immunoprecipitation assay (RIPA) lysis buffer (Cat# 89900, Thermo Fisher Scientific, USA) to each well for 30 min. For antigen detection, the PDMS microchamber of the microarray chip bound GOQDs slides with microprinted antibodies was blocked by 1% BSA for 10 min, then, by applying negative pressure and passing through the flow channels between the microwells, the sEV lysate was transferred to the wells on microarray chip for 40 min of incubation and then the supernatant was removed. For fluorescent labelling, the microarray chip was peeled off in 1% BSA, and the slide was incubated with biotin-containing detection antibody at a final concentration of 10 μg/mL for 45 min, followed by 30 min of incubation with 100× diluted APC-conjugated streptavidin. After thorough washing with 1 × PBS and distilled water, the chip was spun to dry. The fluorescent intensity of antigens was measured using a fluorescence scanner (GenePix Microarray Scanner 4400 A, Molecular Devices LLC, San Jose, CA, USA). Table S2 summarizes all antibodies used for antigen capture and detection and protein standards for calibration.

Cell lines

The immortalized human ovarian surface epithelial cell line (T1074) was purchased from Applied Biological Materials Inc. (Richmond, BC, Canada) and cultured in Prigrow I medium containing 10% fetal bovine serum (FBS; Biological Industries, Beit-Haemek, Israel). Ovarian cancer cell lines SKOV3 cell line and A2780 cell line were purchased from ATCC and Sigma and cultured in Dulbecco's modified Eagle medium (DMEM; Gibco, Grand Island, NY, USA) and RPMI 1640 medium (Gibco, Grand Island, NY, USA), respectively, both of which were supplemented with 10% FBS.

sEV isolation

To obtain sEVs from serum samples, the MagicOmics-EMB Exosomes Enrichment Kit (Qinglianbio, Beijing, Cat# MagicOmics-EMB8×) was used according to the manufacturer's instructions. Briefly, 500 μL serum was mixed with an equal volume of Loading Buffer, and then added 10 μL of Reagent A followed by centrifuging at 3,000 g for 10 min at 4 °C. Transfer 1 mL of the supernatant to a new 1.5 mL centrifuge tube containing equilibrated exosome enrichment magnetic beads (EMB beads). Tubes were incubated on a rotator of 10 rpm for 1 h at room temperature and then were briefly centrifuged. Placed the tubes back on the magnetic separator for 3 min to clarify the liquid and then discarded the

supernatant. The beads were washed by Wash Buffer 1 and 2 sequentially. After the removal of the supernatant, the beads with sEVs were treated with RIPA lysis buffer (Beyotime, Haimen, China) to obtain sEV proteome for the following analysis.

Differential ultracentrifugation was conducted to isolate sEVs from cell lines. In brief, sEVs from different cell lines were obtained from an equal volume of conditioned medium derived from the same number of cells. Specifically, the cells were initially cultured in complete medium until they reached 80% confluence in 15-cm culture dishes. The medium was then replaced with 20 mL of exosome-depleted serum (CELLiGENT, Uruguay) medium per dish, followed by an additional 48-hour incubation period. Finally, a total of 100 mL of conditioned medium was collected from five 15-cm dishes for subsequent sEV isolation. In the differential ultracentrifugation method, sEVs were isolated from the medium through a series of centrifugation steps performed at 4 °C. The initial centrifugation was conducted at 500×g for 15 min, followed by an additional centrifugation at 2,000×g for 10 min to remove dead cells. Cell debris was subsequently eliminated by centrifugation at 10,000×g for 30 min. The sEVs were then pelleted via ultracentrifugation at 110,000×g for 70 min using a Beckman Ti70 rotor. The resulting pellet was resuspended in 1 mL of phosphate-buffered saline (PBS), filtered through a 0.22-μm membrane, and subjected to a final ultracentrifugation at 110,000×g for 70 min to remove soluble serum components and secreted proteins. The sEV pellet was resuspended in an appropriate volume of PBS, and the protein concentration was determined using the bicinchoninic acid (BCA) assay (Thermo Scientific, Cat# 23227). The final concentration of sEV-derived proteins was adjusted to 5 μg/mL for subsequent experiments.

PKH26 sEV staining procedure

The PBS solution containing enriched sEVs were mixed with 100 μL of Diluent C, followed by the addition of 0.4 μL of PKH26 stock solution. The mixture was incubated at 4 °C for 4 min, and the staining reaction was terminated by adding 200 μL of 0.5% BSA. To remove unbound dye, the mixture was centrifuged at 100,000 g for 1 h, and the supernatant containing the dye was discarded. The stained sEVs were resuspended in PBS solution.

Nanoparticle tracking analysis

Nanoparticle tracking analysis was performed using the Nanosight NS 300 system (NanoSight Technology, Malvern, UK), which is equipped with a 488 nm laser and a highly sensitive sCMOS camera. sEVs were diluted 100–500 times to achieve a range of 20–100 objects per frame. After being manually introduced into the sample chamber, each sample was measured in triplicate using a camera level of 13 (acquisition time: 30 s; detection threshold: 7). A minimum of 200 complete tracks were analyzed per video and the analysis was carried out with NTA analysis software version 2.3.

Transmission electron microscopy

sEV pellets were fixed with 2.5% glutaraldehyde at room temperature for 10 min. Subsequently, a 5–10 μL drop of sEV suspension was loaded onto a copper mesh. After removing excess liquid via filter paper, the sEV samples were rinsed three times in PBS for 10 min each. Finally, the sEVs on the grid were negatively stained with 1% uranyl acetate (10 μL) for 1 min and observed using transmission electron microscopy JEM-1400.

Western blot

T1074 cells and sEVs harvested from either cell lines or patients' blood were lysed in RIPA lysis buffer to extract total protein. Protein concentrations were quantified using the BCA protein assay, and 20 μg of protein was loaded into each well for Western blot analysis. Proteins were separated via sodium dodecyl sulfate polyacrylamide gel electrophoresis (SDS-PAGE) and subsequently transferred to poly-vinylidene fluoride (PVDF) membranes through electrical means. After transfer, the membranes were subjected to a blocking process in tris-buffered saline with Tween 20 (TBST) containing 5% skimmed milk for a duration of 2 h, followed by overnight incubation at 4 °C with primary antibodies in the indicated dilution. Following three washes in TBST, the membranes were incubated with 1:1000 diluted horseradish peroxidase (HRP)-conjugated secondary antibody at 37 °C for 1 h. Lastly, protein bands were detected by an enhanced chemiluminescence detection system (Amersham Biosciences). The antibodies used were Anti-CD63 antibody (Abcam, Cat# ab193349), Anti-TSG101 antibody (Abcam, Cat# ab125011), Anti-GM130 antibody (Proteintech, Cat# 66662-1-Ig), Anti-CD9 antibody (Cell signalling Technology, Cat# 13174), Anti-mouse secondary antibody (Proteintech, Cat# RGAM001), and anti-rabbit secondary antibody (Proteintech, Cat# RGAR001). The ECL chemiluminescence solution (Cat# A38554) was purchased from Thermo Fisher.

Mass Spectrometry-based proteomics

For serum samples, 30 μL of lysis buffer was added to each sample well and incubated in a metal bath at 95 °C for 10 min. For enzyme reconstitution, 100 μL of ultrapure water was added to the enzyme vial and thoroughly mixed. Each sample was then supplemented with 100 μL of digestion buffer and 2 μL of the reconstituted enzyme solution. The samples were placed in a preheated shaking incubator at 37 °C, 1000 rpm, for at least 4 h. Following digestion, an eight-strip tube was placed on a magnetic

separator for 10 min until the solution became clear. The supernatant was carefully transferred to a new EP tube. To quench the reaction, 5 μL of quench buffer was added to the new tube and thoroughly mixed, followed by centrifugation at 14,000×g for 10 min. Peptide desalting was performed using a C18 desalting column. The column was activated with 100% acetonitrile, equilibrated with 0.1% formic acid (FA), and loaded with the peptide sample. The column was then washed with 0.1% FA to remove impurities, followed by elution with 70% acetonitrile. The eluate was collected and freeze-dried. The dried peptide samples were reconstituted in 0.1% FA in water and spiked with iRT standard peptides. A total of 1 μg of sample was injected for liquid chromatography-mass spectrometry (LC-MS) analysis. Peptides were separated using a nano-LC system with a C18 analytical column. The chromatographic gradient conditions were as follows: starting at 8%, increasing to 12% over 5 min, then to 30% over 35 min, followed by a gradual increase to 40% at 44 min. The proportion of mobile phase B was then raised to 95% at 45 min and held at 95% until 60 min. The analysis was conducted on a Q Exactive HF-X mass spectrometer (Thermo Fisher Scientific) equipped with a NanosprayFlex™ (ESI) ion source. The ion spray voltage was set to 2.4 kV, and the ion transfer tube temperature was maintained at 275 °C. Data were acquired using the data-independent acquisition (DIA) mode, with a full MS scan range of m/z 350–1500. The mass resolution was set to 60,000 for full MS scans, with a C-trap maximum capacity of 3×10^6 and a maximum ion injection time of 50 ms. Peptide fragmentation was performed using higher-energy collisional dissociation (HCD) with stepped collision energies of 25.5, 27, and 30%.

For cell lines, protein samples were prepared according to previous studies [24, 25]. In brief, sEVs were lysed with RIPA lysis buffer. The suspension was analyzed by SDS-PAGE and Coomassie G-250 (Beijing Wokai Biotechnology Co., LTD, Beijing, China, Cat# D10828) staining. After destaining with water, each lane of each sample was manually cut into eight bands. These cut gels subsequently underwent in-gel digestion and dehydration using a vacuum concentrator. The dried peptides were then reconstituted in 0.1% FA and loaded onto C18 StageTips (Thermo Fisher Scientific, Waltham, USA) conditioned with 50% acetonitrile/0.1% FA. After two washes with 0.1% FA, the peptides were eluted with a solution of 50% acetonitrile and 0.1% FA and dehydrated in a vacuum concentrator. The extracted peptides were analyzed by an Orbitrap Fusion Lumos mass spectrometer (Thermo Fisher Scientific). coupled with an Easy-nLC 1200 UPLC system (Thermo Fisher Scientific). Briefly, these peptides were dissolved in 25 μL of solvent A (0.1% FA in water) and loaded onto a homemade trap column (100 μm × 2 cm) packed with C18 reverse-phase resin (particle size, 3 μm; pore size, 120 Å; SunChrom, USA) at a maximum pressure of 220 bar with 12 μL of solvent A. The sample was subjected to chromatographic separation on a 150 μm × 15 cm homemade silica microcolumn (SunChrom, USA) with a particle size of 1.9 μm and a pore size of 120 Å, using a gradient of 11–95% mobile phase B (80% acetonitrile and 0.1% FA) at a flow rate of 600 nL/min for 30 min. The gradient elution conditions were as follows: 11–13% mobile phase B for 2 min, 13–32% for 16 min, 32–42% for 7 min, 42–95% for 1 min, and 95% for 4 min, for a total of 30 min. MS analysis was performed on an Orbitrap mass analyzer with full scans (350–1,550 m/z) followed by data-dependent acquisition and a mass resolution of 120,000. In top-speed mode, the ions with the highest intensity were isolated in Quadrupole using a 1.6 m/z window and fragmented by higher energy collisional dissociation with a normalized collision energy of 32%. Subsequently, these ions were detected in the Orbitrap at a mass resolution of 15,000, with maximum ion injection times of 50 and 22 ms. The automatic gain control (AGC) targets for full MS and MS/MS were set to 4e5 and 5e4, respectively, while dynamic exclusion time was set to 30 s. Peptide match and isotope exclusion were enabled.

Identification of differentially expressed proteins

To identify differentially expressed proteins between EOC patients and healthy controls, raw gene counts were identified and normalized with HTSeq. Using the "DESeq" package, the corrected p-value < 0.05 and |fold change| > 3 for cell lines and p-value < 0.05 and |fold change| > 1.5 for blood samples were set as the significance criteria, respectively, to identify elevated DEP, which were displayed with volcano plots.

KEGG pathway and gene ontology enrichment analyses

KEGG pathway and Gene Ontology enrichment analyses were performed using the "clusterProfiler" R package to identify functions and pathways enriched among differentially expressed proteins between EOC samples and healthy controls.

EOC diagnostic model construction

The 9-protein model was constructed employing ridge regression through the "glmnet" R package, which included five-fold cross-validation on the training dataset to enhance model validity and performance. Additionally, to assess the model's diagnostic accuracy, a receiver operating characteristic (ROC) curve was generated using the "pROC" R package.

Statistical analysis

Data normality was assessed using the Kolmogorov-Smirnov test, while homogeneity of variance was

evaluated using Levene's test. Normally distributed data were presented as the mean ± standard deviation, while the other data were presented as the median and interquartile range for continuous variables and counts and percentages for categorical variables. The one-way Student *t*-test was used for the comparison of normally distributed data while Mann-Whitney U test for the other continuous data. The consistency between blood- and cell line-derived sEVs proteomes was assessed using Pearson correlation analysis. The linear relationship between fluorescence intensity or optical density (O.D.) values and target antigen concentrations was measured by R-squared (R^2). The p-value < 0.05 was considered statistically significant.

Results

Develop a "one-step" microfluidic platform for sEV capture, in situ lysis, and biomarker detection

To efficiently capture protein features of sEVs and enable high-throughput analysis for early EOC detection, we developed a microfluidic platform. This platform integrates sEVs capture, in situ lysis, and biomarker detection, expanding the analysis scope beyond the sEVs surface. Its performance was validated using a prospectively enrolled EOC case-control cohort. A schematic diagram of the study is shown in Fig. 1.

Due to the scarcity of sEVs in the blood, the power of capturing sEVs is the initial "checkpoint" in evaluating the performance of any sEV-focused microfluidic device. GOQDs have demonstrated their great potential in biosensors, bioimaging, and other biomedical applications [26]. We wondered whether GOQDs could facilitate sEV capture and be suitable for sequentially in situ sEV lysis. As illustrated in the schematic diagram (Fig. 2A), we constructed the sEV-capture microfluidic chip by bonding a sample-loading polydimethylsiloxane (PDMS) chip to a GOQDs-assembled glass slide, allowing for the simultaneous analysis of up to 60 samples. To specifically capture sEVs, CD63 antibodies were used, as they can better differentiate sEVs from other extracellular vesicles [27]. Theoretically, a GOQDs-assembled chip immobilizes CD63 antibodies that bind CD63 on the sEV surface, thereby efficiently trapping sEVs. To examine this hypothesis, we first assessed the distinct concentrations of CD63 antibodies and incubation periods on the chip. Using fluorescent secondary antibodies to label CD63 immobilized on the chip, we demonstrated that the maximum sEV capture capacity of the chip was achieved when the microwell was incubated with 4 μL of 100 μg/mL CD63 antibody for 12 h (Figures S1A, B), which was established as the standard protocol for the sEV microfluidic chip preparation.

To assess the sEV capture power of the GOQDs-CD63 antibody-based microfluidic chip, a series of solutions with varying concentrations of APC-labeled sEVs were introduced into distinct microwells. The captured sEVs were detected using a high-resolution fluorescence scanner and scanning electron microscope (SEM). A linear correlation was observed between the sEV concentrations and fluorescence intensity (Figure S1C). Even at a concentration of 10^3 sEVs/mL, the fluorescence signals of sEVs were detected, which is significantly lower than the concentration of sEVs in serum from healthy individuals and patients with cancers [28]. Consistently, chip-captured intact sEVs were also observed by SEM in all microwells with various sEV concentrations, including 10^3 sEVs/mL (Fig. 2B and Figure S1D). These results indicate that the chip is highly effective in capturing sEVs.

Given that immunoaffinity is also affected by interaction time between antibodies and antigens, we further investigated the optimal incubation time of the sample in the microwells for the maximal sEV capture efficiency of the chip. Considering the sEV concentration in healthy individuals and the counting of sEV fluorescence under high-resolution microscopy, we employed a PKH26-stained sEV suspension with a concentration of 10^9 sEVs/mL. To evaluate the efficacy of sEV enrichment for the chip, we loaded the PKH26-stained sEV solution to several microwells. Once reaching the designated incubation period, the residual eluent was transferred to a new microwell. The microwells prior to and post liquid-transfer were allowed to air dry. Then, we measured the fluorescence signals for sEVs and compared the fluorescence intensities of captured sEVs in the microwell and its corresponding transferred microwell across different incubation durations. As anticipated, with increasing incubation time, more fluorescent signals were detected in the microwells, while the fluorescence signals in the microwells of transferred eluent correspondingly decreased. The fluorescence signals from the incubation microwells reached a plateau after 60 min, where prolonged incubation time did not significantly improve sEV enrichment (83.6% for 60 min vs. 84.1% for 120 min; Fig. 2C). Therefore, 60 min of incubation is suggested for capturing sEVs from human serum samples.

For sEV lysis, the second "checkpoint" of the sEV-capture chip is the efficiency of in situ sEV lysis, which also determines whether there will be sufficient biomarkers in sEV lysate for subsequent investigations. To assess whether sEVs captured in the chip were lysed efficiently, lysis buffer was loaded to the microwells with captured sEVs and sequentially cleaned by the buffer. The reduction of CD63-APC fluorescence signal labelled on sEVs reflected the lysis process. The fluorescent signals of the sEVs weakened over time and vanished after 30 min (Fig. 2D and Figure S1E). This result demonstrated the efficacy of in situ sEV lysis process on the chip and

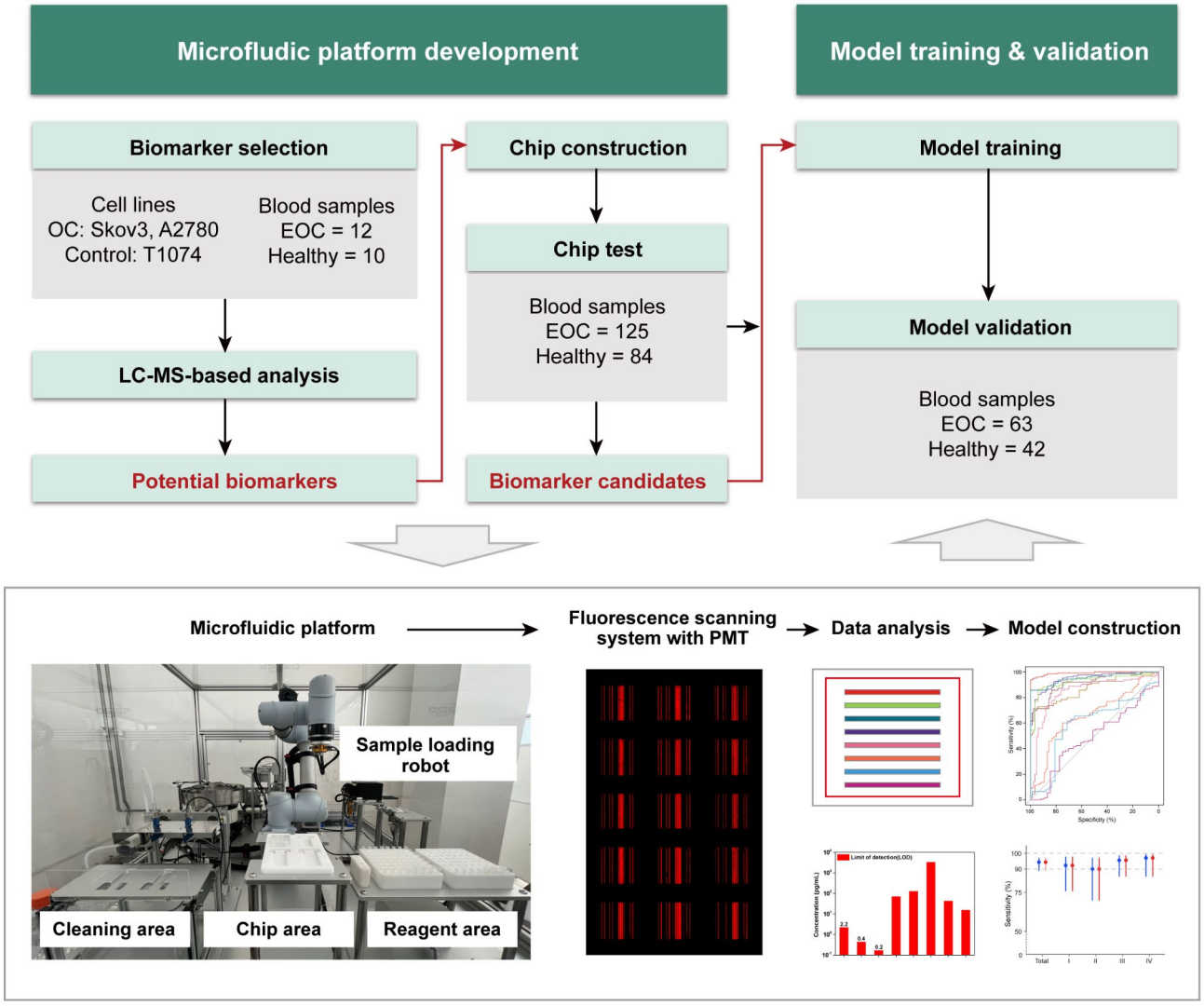

Fig. 1 Schematic diagram for microfluidic platform and study design.
The microfluidic platform mainly contains two functional chips, a microfluidic chip for capturing sEVs and in situ lysis and a microarray chip for targeted sEV-derived protein detection. The sEV-capture microfluidic chip is successively assembled with GOQDs and CD63 antibodies, and the microarray chip is microprinted with antibody microstrip arrays to capture targeted proteins. To detect the target antigens in human blood samples, approximately 2 μL of serum is added to the platform in each microwell, up to 60 samples per test. The sEVs in samples are captured and lysed, and the target biomarker is then assessed on a microarray chip. The amount of target biomarkers is determined based on its fluorescent intensity detected on the chip by a separate scanner. In this study, we constructed an EOC-screening microfluidic platform, with 12 biomarkers identified by analyzing LC-MS proteomes of sEVs harvested from cell lines and human serum. This constructed platform assessed clinical serum samples of a prospective cohort. An EOC early detection model was developed and validated based on the levels of 12 biomarkers in the cohort

suggests the optimal lysis treatment time, approximately 30 min, for future implementation.

To integrate a customizable biomarker detection function into the automatic sEV analysis system, enabling project-specific analyses. Antibodies to specifically capture the target proteins were directly microprinted on the GOQDs-assembled chip and formed a position-encoded microarray chip. Here, we evaluated the biomarker detection performance of the chip by comparing it with a conventional method, ELISA analysis. Explicitly, osteopontin (OPN) monoclonal antibodies were microprinted on the chip, and the antigen solutions of OPN with varying concentrations were added to the chip, whose fluorescent signals were presented as a fine line on the microfluidic chip. As illustrated in Fig. 2E, the intensity decreased in a linear manner with the lowered concentration of the antigen. Intriguingly, the chip detected the antigen at a concentration of 0.02 pg/mL, whereas the limit of detection (LOD) of the ELISA test was 12.29 pg/mL. Notably, there was a considerable difference in the requirement of sample amounts between the microfluidic chip (2 μL) and ELISA (50–100 μL) per test. These findings reflect

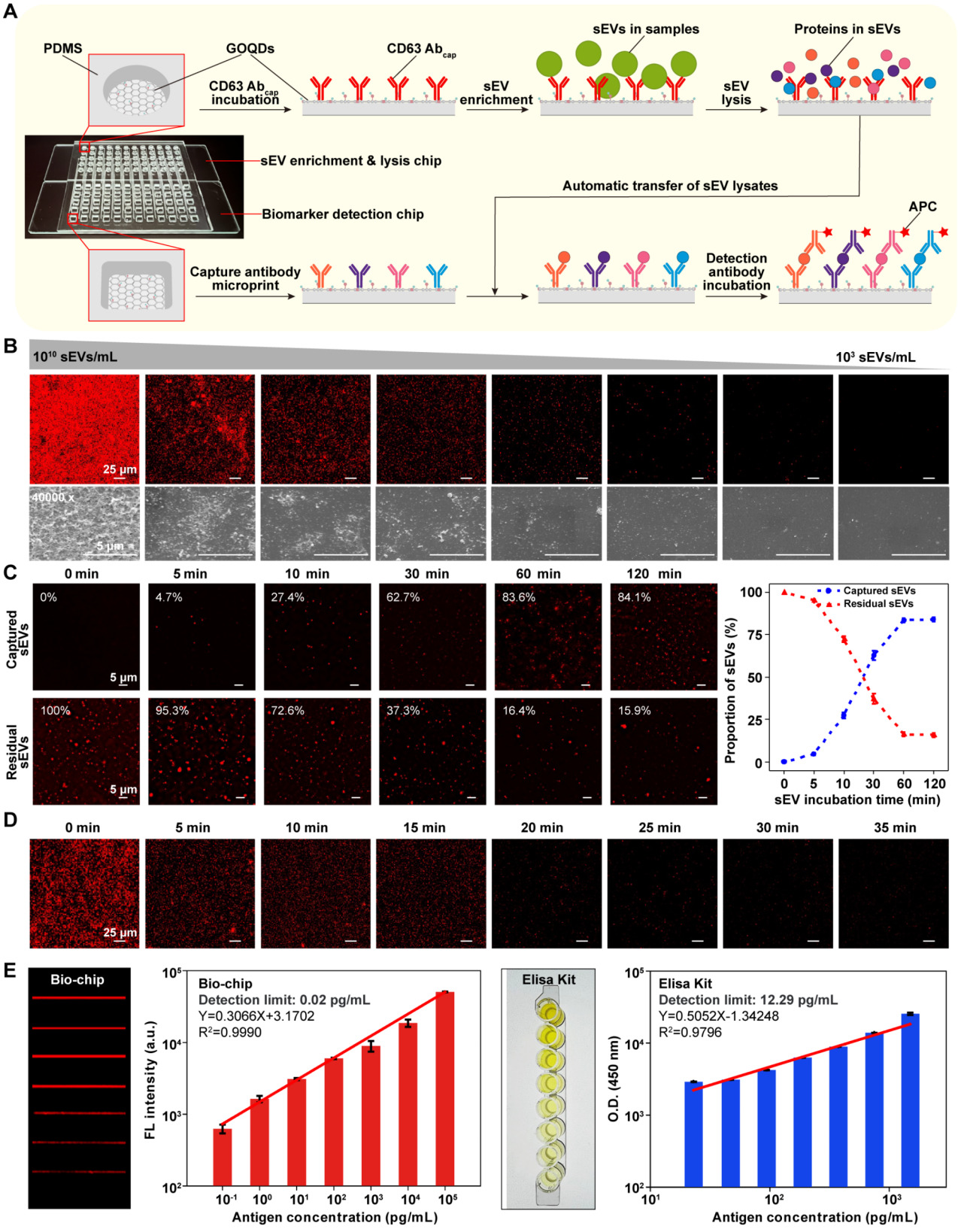

Fig. 2 (See legend on next page.)

(See figure on previous page.)

Fig. 2 Design and validation of microfluidic chips and microarray chips.

A, Design of microfluidic and microarray chips. The microfluidic chip for sEV capture and lysis was comprised of a glass slide assembled with GOQDs and a 60-well PDMS microchamber layer, allowing for the simultaneous analysis of up to 60 samples per test. CD63 antibody solution was used as sEV capture solution in this study, which was added to every microwell on the chip and CD63 antibodies would be immobilized by GOQDs with incubation. After washing off extra antibodies with DPBS buffer, the chip was added with liquid samples containing sEVs and incubated for sEV enrichment. After thoroughly washing with DPBS buffer, captured sEVs were lysed with lysis solution. Then, the lysate of each sample was automatically transferred from the microfluid to a distinct microwell on a microarray chip for target antigen detection by applying negative pressure through the flow channels between the microwells. On the other hand, a microarray chip for antigen detection was also fabricated on a GOQDs-assembled glass slide substrate with a 60-well PDMS microchamber layer. The antibodies targeting biomarkers of interest were previously defined and microprinted on the GOQDs slide as a position-encoded array, each of whose unit contained a certain number of microstrips to specifically capture corresponding biomarkers. Once target biomarkers immobilized from liquid samples, such as sEV lysate, a cocktail solution of biomarker detection antibodies was loaded and well covered the whole chip. With removing unbonded antigens with DPBS buffer, fluorescence intensities of the detection antibody targeting each biomarker were detected to calculate the level of biomarkers in each sample.

B, Qualitative validation of microfluidic chips for sEV capture. A serial of sEV solution with concentration gradients (10^{10} sEVs/mL to 10^{3} sEVs/mL) was added to the chip. The captured sEVs on the chip were detected by fluorescent staining of APC-labelled CD63 antibodies (upper panel) and SEM (lower panel, 40,000× magnification).

C, Qualitative validation of microfluidic chips for sEV enrichment efficiency. A solution of PKH26-labelled sEVs at 10^{9} sEVs/mL was loaded onto the chip for validation. When reaching the set incubation times, the solution was transferred to a new microwell. The number of PKH26-labelled sEVs was counted in 3 areas (100 μm × 100 μm) randomly selected in each well.

D, sEV lysis efficiency analysis. sEVs were labelled by CD63-APC and treated with 5 μL lysis solution on the slice for different treatment time.

E, Comparison of antigen detection between microarray chip and traditional ELISA assay. The left panel is the fluorescent image of the chip. The OPN antigen was diluted according to a 10-fold gradient concentration. The fluorescence values were quantified to be fitted to a linear curve. LOD for each antigen was calculated

not only the precision of the chip but also a significantly lower demand for the sample amount for analysis using the chip. Given the clinical reality of limited patient samples, this chip could fulfil essential clinical test requirements without an additional burden.

Differential abundance of sEV-derived proteins in patients with EOC and healthy individuals revealed candidate biomarkers for diagnosis

To identify the ovarian cancer biomarkers carried in sEVs, we used prospectively collected blood samples to capture the signals of patients' status and cell lines reflecting the stable features of EOC. We conducted proteomic analyses on sEVs from patients with EOC and ovarian cancer cell lines. (Fig. 1 and **Methods**). To harvest sEVs, we retrieved the blood samples from 12 patients with EOC and 10 healthy individuals and culture supernatant from cell lines of Skov3 (ovarian serous cystadenocarcinoma), and A2780 (ovarian endometroid adenocarcinoma), and T1074 (ovarian epithelial cells, for control). After collecting sEVs from patients' serum and cell culture extracellular fluid, the morphology of collected particles was examined by transmission electron microscope (TEM). sEVs in all samples demonstrated the presence of rounded, cup-shaped, and double membrane-bound vesicle-like structures (Fig. 3A). Moreover, nanoparticle tracking analysis (NTA) exhibited the majority of the particles ranging from 100 to 200 nm in both patients' serum and cell lines, suggesting that the collected particles were mainly sEVs (Fig. 3B). To further assess the purity of the collected sEVs, western blot analysis was performed targeting three sEV-specific markers, CD63, CD9, and TSG101 (tumor suppressor gene 101). Additionally, GM130, a Golgi marker, was included as a negative control to confirm the absence of cellular contamination. This analysis confirmed the collection of sEVs from both patients with EOC and cell lines (Fig. 3C).

Implementation of mass spectrometry-based proteomic analysis, approximately 3629 and 1088 proteins were identified from EOC cell lines and patients' serum, respectively (Tables S3, S4). Data visualization of these proteins was demonstrated in a heatmap (Fig. 3D). A two-dimensional scatterplot of principal component analysis (PCA) revealed that the sEV proteomic profiles of patients with EOC generally were clustered apart from those of healthy individuals (Fig. 3E), consistent with the observation in cell lines (Fig. 3F). Furthermore, Pearson correlation analysis indicated that protein levels do not seem to correlate between these two sourses ($r = 0.064$, $p = 0.12$; Fig. 3G).

To screen for EOC-associated proteins, we identified 332 and 1321 differentially upregulated proteins of sEVs from blood samples and cell lines, respectively, compared to their corresponding healthy controls (Fig. 3H). We observed 75 elevated proteins that were shared between EOC cell lines and patients (Fig. 3I). The KEGG pathway enrichment analysis demonstrated these proteins involved in platelet activation, intercellular junctions, various degenerative diseases, etc. (Fig. 3J). These findings are consistent with previous studies [29]. Given the low Pearson correlation between patients and cell lines as shown above, to better capture sEV proteome signatures, we collectively explored EOC-associated biomarkers from 3 sources: (1) the top 20 upregulated proteins in two EOC cell lines, (2) the top 20 upregulated proteins in patient serum samples, and (3) proteins enriched in the

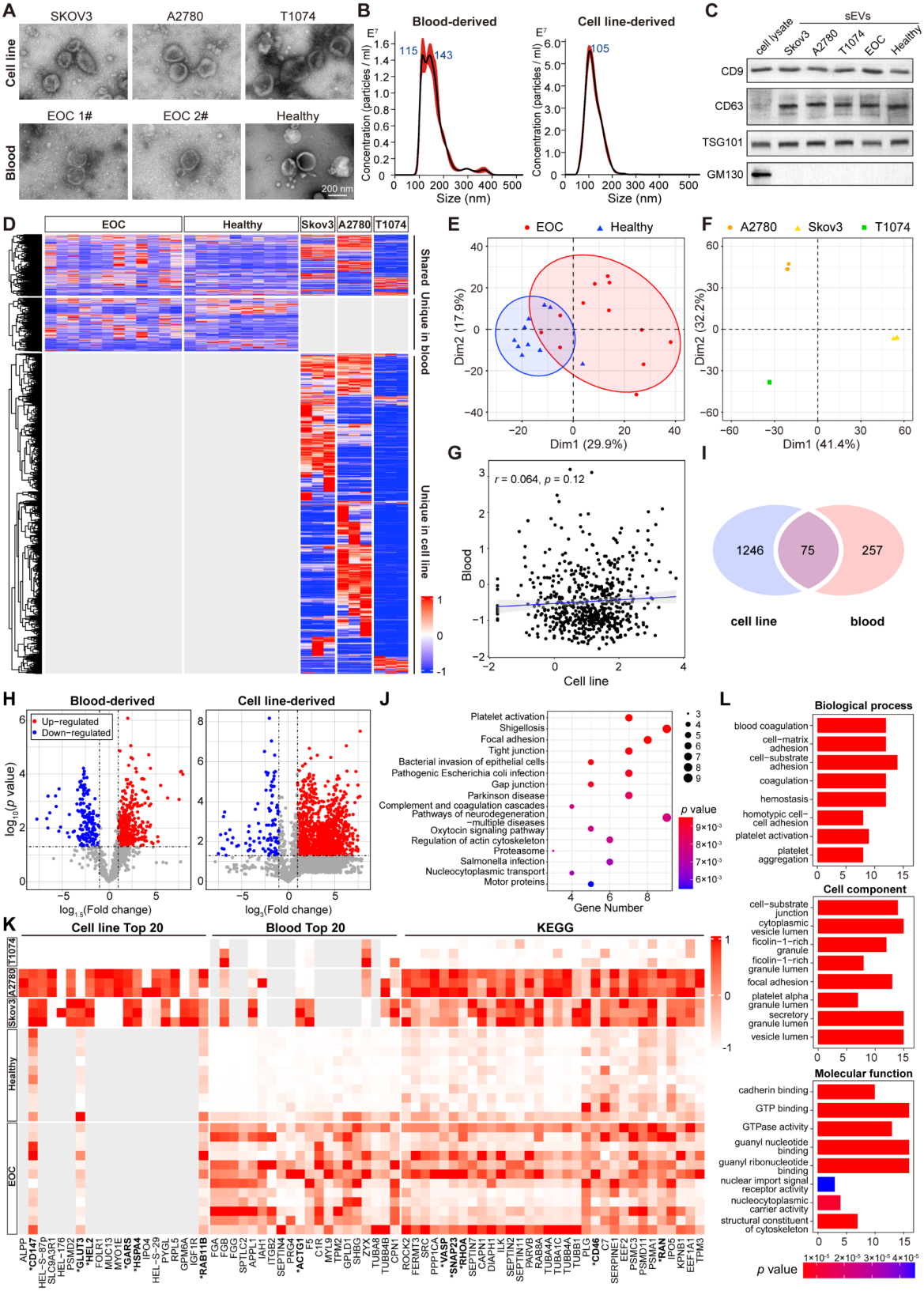

Fig. 3 (See legend on next page.)

(See figure on previous page.)

Fig. 3 Proteomic analysis of sEVs harvested from EOC cell lines and patients' blood.
A, sEVs isolated from cell line culture supernatant and human blood.
B, Nanoparticle tracking analysis of the size distribution and concentration for sEVs from cell lines and human blood.
C, Western blot analysis was performed targeting three sEV-specific markers, CD9, CD63, and TSG101 in the cell lysate of T1074 cells and sEVs harvested from cell lines and human serum. The Golgi marker GM130 was used as a negative marker to assess cellular contamination.
D, Heatmap of differentially expressed proteins among EOC patients, cell lines, and healthy controls. Color scale ranges from red to blue representing protein levels from high to low. Proteins unidentified in the sample are shown in grey.
E, PCA analysis of proteomic profiles of sEVs isolated from blood samples of 12 patients with EOC and 10 healthy controls.
F, PCA analysis of proteomic profiles of sEVs of two EOC cell lines and a control cell line.
G, Pearson correlation analysis of sEV protein levels between blood samples and cell lines.
H, Volcano plots of DEP in EOC patients and cell lines compared with their respective healthy controls.
I, Venn diagram showing the overlap between blood samples and cell lines and all the sEV proteins identified in these two resources by LC-MS.
J, KEGG enrichment analysis of 75 proteins elevated in sEVs derived shared between EOC patients and cell lines.
K, Heatmap of elevated proteins for EOC detection biomarker exploration, including the respective top 20 highly expressed proteins in EOC cell lines and patients and shared elevated proteins excluding those enriched in KEGG pathways of multiple neurodegenerative diseases. Color scale ranges from red to blue representing protein levels from high to low. Proteins unidentified in the sample are shown in grey.
L, GO enrichment analysis of the proteins described in (**K**)

above KEGG pathways except for multiple neurodegenerative diseases. A total of 72 proteins, enriched in platelet activation, cell-substrate junctions, cadherin binding, vesicle lumen, etc., were selected as a pool of EOC potential biomarkers for further investigation. The expression levels of these proteins were summarized in a heatmap (Figs. 3K, L).

Develop customized EOC biomarker detection microarray chip

As described above, the biomarker detection chip of this microfluidic platform is designed to accommodate custom biomarker-capture antibodies for microprinting. Here, we use commercialized antibodies, the most common and convenient source of antibodies for most studies. Of the 72 initially identified proteins, 12 were selected for further analysis based on the availability of commercial paired antibodies (capture and detection antibodies) that recognize distinct epitopes without steric hindrance, as well as corresponding recombinant proteins for quantitative calibration. These biomarker-capture antibodies were microprinted onto the GOQDs-assembled substrate as a microstrip array. The antibody barcode microarray of these 12 antibodies was integrated with a 60-microwell PDMS chip, where each microwell contained a unit of 12 microstrips, one microstrip per target biomarker. This setup allows the simultaneous analysis of 12 biomarkers for 60 samples in a single run. Before detection, the fluorescent secondary antibody IgG-AF488 was added to microstrips lying out of the detection zoom to assess whether biomarker-specific capture antibodies had been immobilized on the GOQD chip. Only microstrips with immobilized antibodies displayed fluorescence. The microarray chip with the microstrip pattern is demonstrated in Fig. 4A. To ascertain the detection performance of this antibody-microprinted microarray, concentration gradient solutions for each of the protein standards of these 12 antigens were prepared and loaded into distinct wells on microprinted chips, thereby determining the specificity, sensitivity and the LODs for each sEV-capture antibody. With the corresponding biomarker-detection antibody, fluorescent signals were detected only in the microprinted lines of the antibody corresponding to the loaded antigens, thereby confirming the reliability of the chip in simultaneously detecting multiple biomarkers (Figure S3). Consistently, quantitative assessment of fluorescently labeled detection antibody for each biomarker with standards showing that the fluorescence intensity was linearly correlated with antigen concentrations for all the selected antibodies, with correlation R^2 ranging from 0.925 (VASP) to 0.9990 (RAB11B) (Fig. 4B). The LOD of each antibody is shown in Table S5. The lowest LOD (0.02 pg/mL) was observed in RAB11B, which reflects the precision of this chip. Collectively, the above results indicate that the microprinted chip of 12 antibodies could quantitatively analyze EOC biomarkers in patients' serum.

Construct the integrated sEV-based microfluidic platform for EOC biomarker detection

Based on the performance of the microfluidic chip for sEV capture and lysis, as well as the microarray chip for the detection of 12 EOC biomarkers, we developed an integrated sEV-based microfluidic platform for EOC biomarker detection.

To evaluate the overall performance of the platform as a potential EOC sEV detection device for clinical utility, we used a cohort of serum samples from 125 EOC patients and 84 healthy controls (Table S1). Their serum samples were loaded into the ready-to-use sEV-capture microfluidic chips for sEV capture and lysis. Then respective sEV lysates were transferred to distinct microwells of a microarray chip for biomarker capture. The APC-labeled detection antibody cocktail was loaded onto the whole chip to identify the captured biomarkers of interest. The fluorescence intensity of each biomarker per sample was

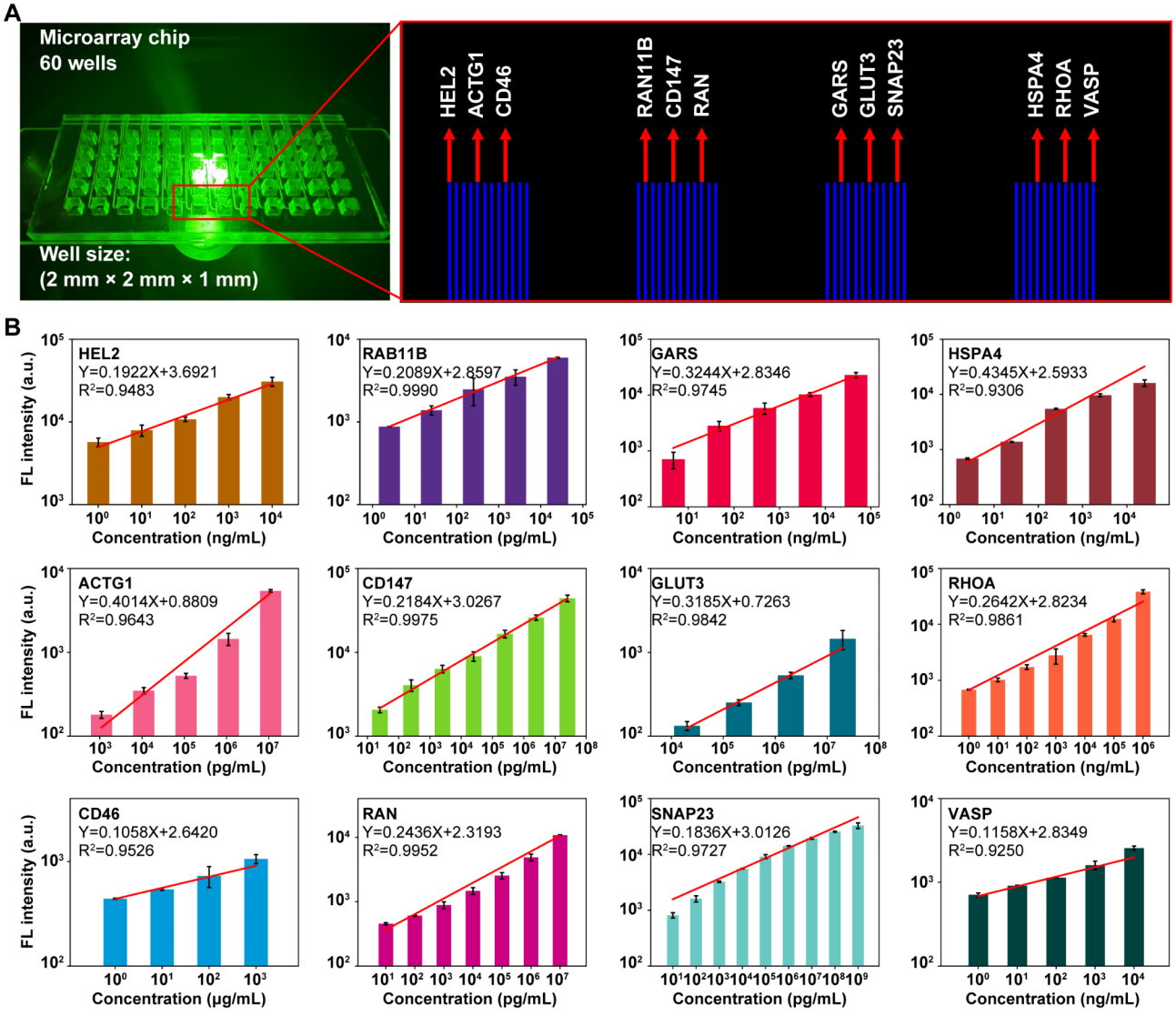

Fig. 4 Construction and validation of microarray chip customized for EOC detection.
A, Photograph of a microarray chip. Blue lines were non-detection ends of the 12-biomarker capture antibody for each microwell on the chip, labeled with fluorescent secondary antibody IgG-AF488 for pre-detection quality control.
B, Quantitative validation of microarray chips in detecting 12 EOC biomarkers. Each antigen was diluted according to a 10-fold gradient concentration. The fluorescence values were quantified and fitted to a linear curve. LOD for each antigen was calculated

detected simultaneously (Figure S4A). Distinct clusters of patients and controls were also observed based on the levels of 12 biomarkers (Figure S4B). As demonstrated in Figs. 5 and 9 out of the 12 biomarkers (HEL2, RAB11B, HSPA4, ACTG1, CD147, GLUT3, RHOA, CD46, and RAN) exhibited higher signals in the majority of EOC patients compared with healthy controls (Figure S4C). In contrast, we did not detect SANP23 and VASP in most patients with EOC and controls. The average concentration of sEV proteins in patients and the overall LOD of each antibody were calculated collectively. Notably, the LOD of GARS was higher than its respective average concentration in serum sEVs (Fig. 5). Consequently, these three biomarkers were excluded to ensure more accurate prediction, resulting in nine candidate biomarkers. These results also demonstrate the efficacy of the integrated microfluidic platform for capturing adequate sEVs with efficient lysis to provide sufficient targeted protein biomarkers for future analyses.

EOC diagnostic model development and validation

The conventional biomarkers currently used for EOC diagnosis, CA125 and HE4, are not optimal, which exhibit relatively low specificity and sensitivity [30]. With this microfluidic platform, we attempted to develop an EOC detection model based on the expression levels of the 9 biomarkers from the aforementioned 125 EOC patients and 84 healthy controls, as a training set. To

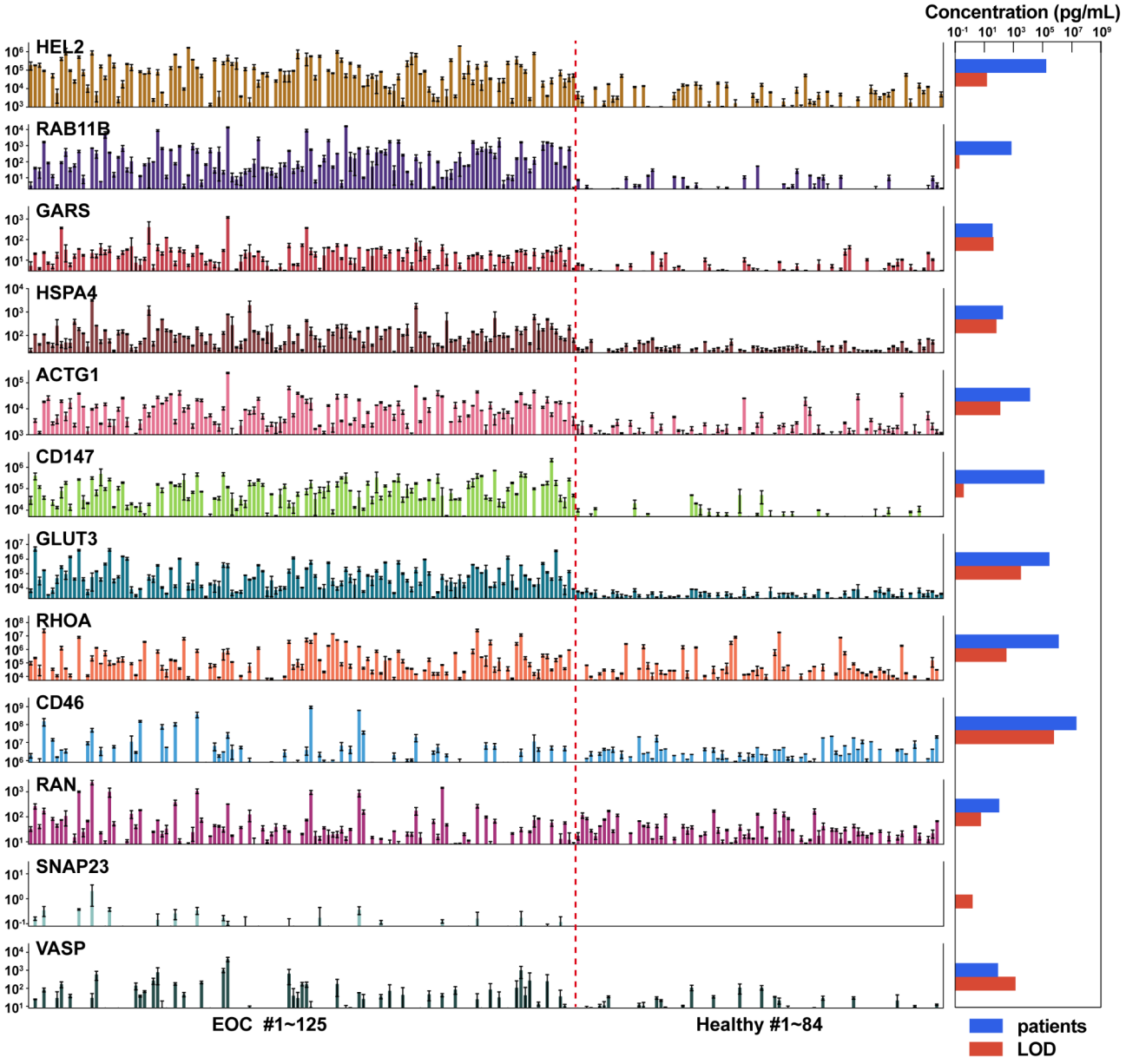

Fig. 5 Using the microfluidic platform to detect the expression levels of 12 EOC biomarkers in serum sEVs from a prospective cohort. The expression level of 12 EOC biomarkers in 125 patients with EOC and 84 healthy controls. Data are presented as mean ± standard deviation of three replicates. For each biomarker, the LOD and the average concentration of EOC patients are graphed on the right

predict EOC in this training set, an area under the curve (AUC) of the receiver operating characteristic curve (ROC) for each biomarker ranged from 0.488 (RAN; 95% CI, 0.408–0.568) to 0.950 (GLUT3; 95% CI, 0.921–0.979) (Fig. 6A). Additionally, we constructed a model (referred to as P9) by combining all 9 candidate biomarkers. This model exhibited an AUC of 0.991 (95% CI, 0.981–1.00), which was higher than the AUC of any single biomarker (Fig. 6A). The sensitivity of the P9 model was 94.4% (95% CI, 88.9–97.3%) at a specificity of 98.8% (95% CI, 93.6–99.8%). Furthermore, we evaluated the performance of the P9 model at different FIGO stages of EOC. The sensitivity was 92.3% (95% CI, 75.9–97.9%) for stage I, 90.0% (95% CI, 69.9–97.2%) for stage II, 95.6% (95% CI, 85.2–98.8%), and 97.1% (95% CI, 85.1–99.5%) (Fig. 6B). High-grade serous carcinoma (HGSC) is the most prevalent type of EOC and is challenging to diagnose at its early stages. The sensitivity of the P9 model reached 88.9% (95% CI, 71.9–96.1%) for the early stage (stage I–II) and 96.5% (95% CI, 88.1–99.0%) for the advanced stage (stage III–IV). (Figure S5A).

To validate the performance of the P9 model, we used another set of 63 patients with EOC and 42 healthy controls. The expression of each of the 12 biomarkers was

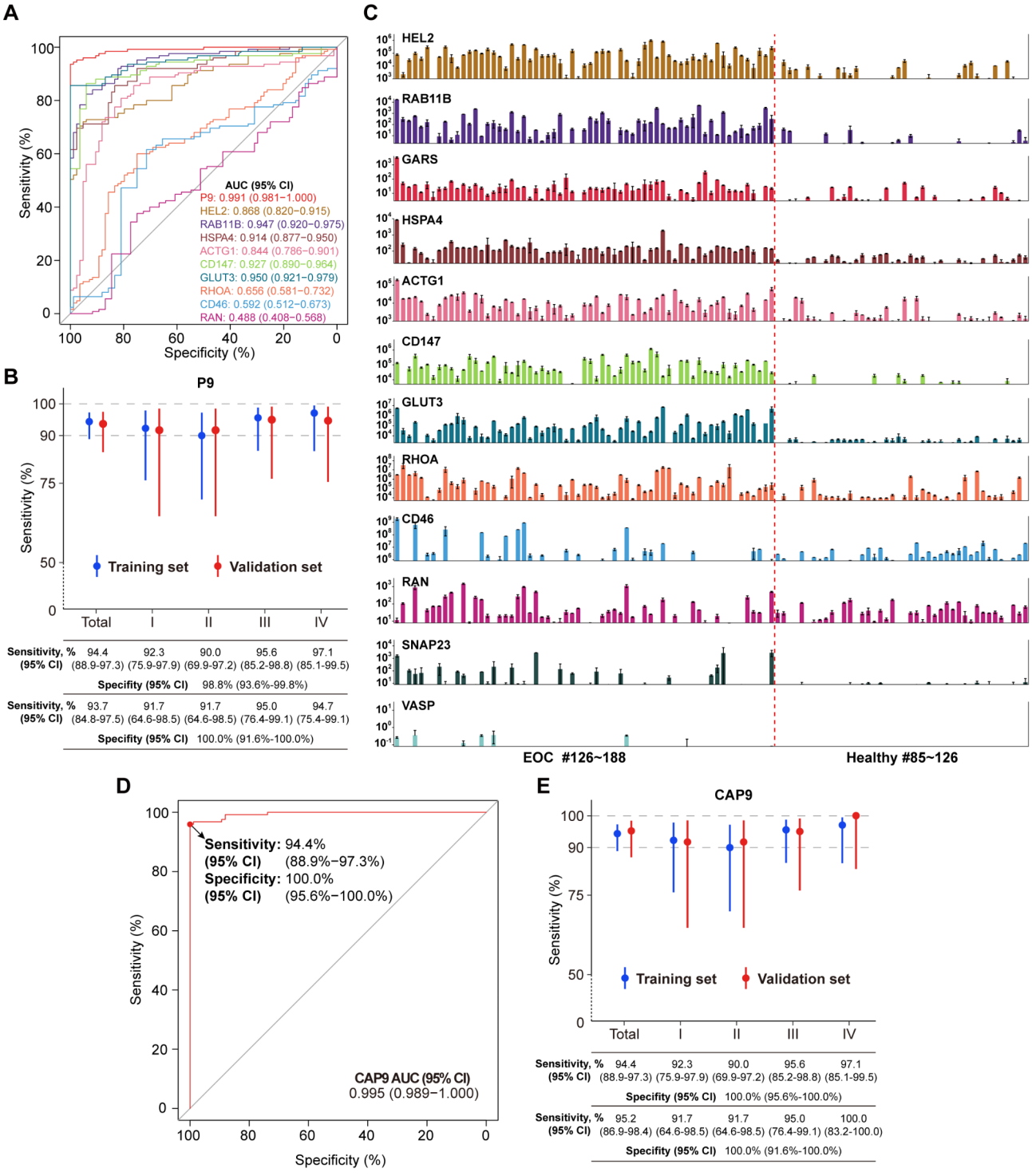

Fig. 6 Construction and validation of EOC detection models.
A, ROC of each biomarker and their combination (P9) for prediction of EOC in the training set.
B, Performance of P9 model, total and stage-wise in both training and validation sets.
C, Expression level of 12 EOC biomarkers in a validation set of 63 patients with EOC and 42 healthy controls. Data are presented as mean ± standard deviation of three replicates. For each biomarker, the LOD and the average concentration of EOC patients are graphed on the right.
D, ROC of the model combining the expression levels of all 9 biomarkers in serum sEVs and the level of CA125 in human blood.
E, Performance of CAP9 model, total and stage-wise in both training and validation sets

obtained (Fig. 6C). The overall expression patten of the 12 biomarkers in this held-out group resembles that in the training set. The sensitivity of the P9 model in the validation set was 93.7% (95% CI, 84.8–97.5%) when the specificity reached 100.0% (95% CI, 91.6–100.0%) and the sensitivity was 91.7% (95% CI, 64.6–98.5%) for stage I, 91.7% (95% CI, 64.6–98.5%) for stage II, 95.0% (95% CI, 76.4–99.1%) for stage III, and 94.7% (95% CI, 75.4–99.1%) for stage IV (Fig. 6B), and the specificity of the P9 model was 89.5% (95% CI, 68.6–97.1%) for stage I–II of HGSC and 93.1% (95% CI, 78.0–98.1%) (Figure S5A).

Given the CA125 cut-off as the current EOC clinic biomarker, we used the CA125 with a fixed cut-off of 35 U/mL to predict EOC in the training set. The AUC of CA125 was 0.910 (95% CI, 0.871–0.948) and when specificity was 78.6% (95% CI, 68.7–86.0%), a sensitivity was 85.6% (95% CI, 78.4–90.7%) (Figure S5B). Visualizing the predictions of EOC positives and negatives of EOC made by CA125 and P9 model separately, only 1 control was identified as EOC positive by the P9 model versus 18 false positives by CA125 solely, so that 17 (94.4%) false negatives of CA125 were correctly predicted by the P9 model. Additionally, only 1 patient was not correctly predicted by CA125 or P9 models (Figure S5C). Therefore, the P9 model could dramatically increase prediction accuracy for both EOC and non-EOC populations. Given that a model based on the CA125 value, rather than a cut-off, showed better performance, we developed a CAP9 model combining the CA125 value and 9 biomarkers, whose AUC surpassed that of the P9 model (Fig. 6D). As shown in Fig. 6E, the specificity of the CAP9 model reached 100.0% in both training and validation sets and higher sensitivity in stage I and IV in the validation set. These findings indicate that an EOC diagnostic model based on the levels of nine sEV-derived biomarkers identified and measured by our integrated platform may benefit patients with EOC by enabling early detection with minimal false positives, particularly when combined with CA125.

Discussion

Invasiveness and high false positive rates have been reported as the main concerns for current large clinical trials of EOC screening. New approaches could be the solution for it. Tumor-derived sEVs have long been recognized as a promising modality for cancer early detection, with their utility demonstrated in several types of cancer [31]. Despite advancements in microfluidic devices for cancer diagnosis based on sEV proteomes, the devices continue to target the antigens on the sEV surface, rather than the cargos inside sEVs, which could severely undermine the significance and potential of the various cargoes inside the sEVs [23, 32]. In this study, we developed a microfluidic platform integrating a microfluidic chip for "sEV capture and lysis" and a microarray chip for "sEV cargo of interest detection and analysis" for EOC early detection in prospectively collected EOC blood samples. Based on EOC biomarker levels detected by the "one-step" microfluidic platform, we developed an EOC diagnostic model, whose performance surpassed that of the conventional serum EOC biomarker, CA125.

To develop the microfluidic and microarray platform, we used the glass-slices assembled with nano-material GOQDs, which have been demonstrated as good substrates for high-efficient antibody immobilization [33]. Sample-loading PDMS chip with detection units bound to the GOQDs chip allows the device to simultaneously process serum samples of up to 60 individuals and 12 biomarkers per sample. Meanwhile, we simplified the recipe of sEV capture antibodies by only targeting CD63, since CD63 has been reported not only to be more sEVs specific but also overexpressed in OC [34]. The consequent sEV capture and enrichment analyses have proved the high efficiency of sEV capture of microfluidic chips with the sole CD63 antibody. The proposed platform is a universal tool to analyze sEV-derived proteins in different diseases, organoids or other research systems. More importantly, for the first time, this microfluidic platform realized sEV collection, in situ sEV lysis, and sEV-derived protein screening with extremely small sample volumes. In addition, these sEV capture and lysis microarray chips were stable at − 80 °C for 10 months at aspects of structure and function, which allows for their promising application.

To calibrate the fluorescent intensity of antibodies printed on the microarray chips, the commercialized protein standards were used, and its LOD was predicted accordingly. However, 3 out of 12 proteins showed quite low levels of expression when analyzing blood samples in the microfluidic platform, whose LODs were higher than their average protein levels in the samples. This could be due to differences in methods, immunofluorescence versus mass spectrum. Meanwhile, these low expression levels were consistent among the samples in both training and validation sets, where the microfluidic and microarray chips were produced at different times, reflecting the robustness of the microfluidic platform. Certainly, the cause of this discrepancy is worthy of consideration and can be avoided by a pre-test. The 9 proteins used to construct the EOC diagnostic model have been reported in several types of cancer, except for HEL2, an E3 ubiquitin-protein ligase. It has been reported to play a key role in ribosome quality control [35], while the direct link of HEL2 to cancer remains unclear, which might be worthy of future investigation. As a factor closely related to the cancer hallmark, the Warburg effect, GLUT3 have been reported in a variety of cancer types [36] but has not yet been reported as a biomarker in sEVs. In this study, we

noticed that the sensitivity of GLUT3 was 85.6% (95% CI, 78.4–90.7%) at a specificity of 100.0% (95% CI, 95.6–100.0%) in the training set, showing its great potential in cancer diagnosis.

Furthermore, based on the expression level of 9 proteins detected by this microfluidic platform, we constructed an EOC diagnosis model, P9, the sensitivity of which was 99.4% (95% CI 88.9–97.3%) at a specificity of 98.8% (95% CI, 93.6–99.8%). In the validation set, the specificity reached 100.0% (95% CI, 91.6–100.0%) with 93.7% (95% CI, 84.9–97.8%) sensitivity. The model's performance in the training and validation sets reflects the robustness and reliability of our non-invasive "one-step" EOC detection microfluidic platform, which is much higher than those of CA125 in our studies, while the performance of CA125 in EOC detection in our study already showed better performance than those reported previously [37]. The high specificity of the P9 model can systematically reduce false positives. To assess the possibility of integrating the P9 model into the current clinic operation, the training cohort was predicted using the model and the sole CA125 cut-off (35 U/mL). We observed extremely high accuracy when test results were concordant in both methods. However, when results differed, the proportion of false results was much smaller in the P9 model, thereby providing a meaningful reference for diagnosis. The model of combined CA125 value and P9 biomarkers reached 100.0% specificity. Given the limited sample size in this study, a larger cohort is needed to further evaluate this combined model.

The occult nature of ovarian cancer is the main reason for most patients with EOC are diagnosed at advanced stages. Liquid biopsy has been developed rapidly for biomarker detection and the amount of sample has been a long concern for both medical personnel and patients, particularly for blood samples [38, 39]. Inevitably, an inadequate sample can lead to questionable results such as false negative. However, patients under certain physiological conditions are not suitable for blood drawn. In this scenario, the dilemma of whether the test will benefit or harm the patient must be addressed. In our study, we used approximately 2 μL of serum per patient and tested for 12 biomarkers as needed, which significantly lowered the sample burden for more tests to benefit patients. With a proper schedule of medical examinations, no extra samples will be required from patients to conduct the test. The volume of serum samples makes this microfluid platform an ideal candidate for clinical tests in the real world. In addition, the cost of the test for each individual is less than that of a conventional CA125 test. Therefore, this EOC early detection test could be suitable for integration into clinical operations in the future.

Conclusions

In conclusion, this study introduced a one-step high-throughput sEV-based microfluidic platform, customized for effective EOC detection with low requirement of serum volume and cost. Our findings also demonstrate the great potential of the platform for other clinical applications by targeting their sEV cargos.

Supplementary Information

The online version contains supplementary material available at https://doi.org/10.1186/s12951-025-03348-4.

Supplementary Material 1: Figure S1–S4, Table S1–S2, Table S5

Supplementary Material 2: Table S3

Supplementary Material 3: Table S4

Acknowledgements

Not applicable.

Author contributions

M.L., L.H., and H.G. conceptualized the study and designed the overall project. Y.W., Y.G., and C.W. conducted experiments and analyzed data. P.W. and W.Y. assisted in sample preparation and data collection. M.L., L.H., H.G., and Yu Z. contributed to the design of the microfluidic platform. Yunhong Z., Xue Z. and Z.L. assisted with the microfluidic platform optimization. Y.W., Y.G., C.W., and Xin Z. prepared the manuscript. M.L., L.H., and H.G. supervised all aspects of the study. All authors reviewed, edited and/or advised on the paper.

Funding

This study was funded by the National Natural Science Foundation of China (NSFC) (T2225006 to M.L., T2488301 to M.L. and 82272948 to M.L.), the National Key R&D Plan of China (2023YFB3210400 to L.H.), and Beijing Municipal Natural Science Foundation (Key program Z220011 to M.L.).

Data availability

The datasets supporting the conclusions of this article are available in the ProteomeXchange repository, PXD053690 (http://www.proteomexchange.org), and in the iProX repository, IPX0009124000 (http://www.iprox.org).

Declarations

Ethics approval and consent to participate

All human materials used in this study were approved by the Medical Science Research Ethics Committee of Peking University Third Hospital (IRB00006761-M2019291). All participants voluntarily signed a declaration of informed consent for participation.

Consent for publication

Written informed consent for publication was obtained from all participants.

Competing interests

The authors declare no competing interests.

Author details

[1]State Key Laboratory of Female Fertility Promotion, Center for Reproductive Medicine, Department of Obstetrics and Gynecology, Peking University Third Hospital, Beijing 100191, China
[2]Institute of Marine Science and Technology, Shandong University, Qingdao 266237, China
[3]School of Integrated Circuits, Shandong University, Jinan 250100, China
[4]National Clinical Research Center for Obstetrics and Gynecology, Third Hospital, Academy for Advanced Interdisciplinary Studies, Peking University, Beijing 100871, China
[5]Key Laboratory of Assisted Reproduction (Peking University), Ministry of Education, Beijing 100191, China

[6]Beijing Key Laboratory of Reproductive Endocrinology and Assisted Reproductive Technology (Peking University Third Hospital), Beijing 100191, China
[7]Department of Radiation Medicine, School of Basic Medical Sciences, Peking University Health Science Center, Beijing 100191, China

Received: 16 December 2024 / Accepted: 23 March 2025
Published online: 07 April 2025

References

1. Lheureux S, Braunstein M, Oza AM. Epithelial ovarian cancer: evolution of management in the era of precision medicine. Cancer J Clin. 2019;69(4):280–304.
2. Reid BM, Permuth JB, Sellers TA. Epidemiology of ovarian cancer: a review. Cancer Biol Med. 2017;14(1):9–32.
3. Farley J, Ozbun LL, Birrer MJ. Genomic analysis of epithelial ovarian cancer. Cell Res. 2008;18(5):538–48.
4. Yarmolinsky J, Bull CJ, Vincent EE, Robinson J, Walther A, Smith GD, et al. Association between genetically proxied Inhibition of HMG-CoA reductase and epithelial ovarian cancer. JAMA. 2020;323(7):646–55.
5. Menon U, Gentry-Maharaj A, Burnell M, Singh N, Ryan A, Karpinskyj C, et al. Ovarian cancer population screening and mortality after long-term follow-up in the UK collaborative trial of ovarian cancer screening (UKCTOCS): a randomised controlled trial. Lancet. 2021;397(10290):2182–93.
6. Buys SS, Partridge E, Black A, Johnson CC, Lamerato L, Isaacs C, et al. Effect of screening on ovarian cancer mortality: the prostate, lung, colorectal and ovarian (PLCO) cancer screening randomized controlled trial. JAMA. 2011;305(22):2295–303.
7. Pinsky PF, Zhu C, Skates SJ, Black A, Partridge E, Buys SS, et al. Potential effect of the risk of ovarian cancer algorithm (ROCA) on the mortality outcome of the prostate, lung, colorectal and ovarian (PLCO) trial. Int J Cancer. 2013;132(9):2127–33.
8. Drescher CW, Shah C, Thorpe J, O'Briant K, Anderson GL, Berg CD, et al. Longitudinal screening algorithm that incorporates change over time in CA125 levels identifies ovarian cancer earlier than a Single-Threshold rule. J Clin Oncol. 2012;31(3):387–92.
9. Kalluri R, LeBleu VS. The biology, function, and biomedical applications of exosomes. Science. 2020;367(6478).
10. Rajagopal C, Harikumar KB. The origin and functions of exosomes in cancer. Front Oncol. 2018;8:66.
11. Zhang X, Yuan X, Shi H, Wu L, Qian H, Xu W. Exosomes in cancer: small particle, big player. J Hematol Oncol. 2015;8:83.
12. Li X, Li C, Zhang L, Wu M, Cao K, Jiang F, et al. The significance of exosomes in the development and treatment of hepatocellular carcinoma. Mol Cancer. 2020;19(1):1.
13. Melo SA, Luecke LB, Kahlert C, Fernandez AF, Gammon ST, Kaye J, et al. Glypican-1 identifies cancer exosomes and detects early pancreatic cancer. Nature. 2015;523(7559):177–82.
14. Li W, Liu JB, Hou LK, Yu F, Zhang J, Wu W, et al. Liquid biopsy in lung cancer: significance in diagnostics, prediction, and treatment monitoring. Mol Cancer. 2022;21(1):25.
15. Nakamura K, Zhu Z, Roy S, Jun E, Han H, Munoz RM, et al. An Exosome-based transcriptomic signature for noninvasive, early detection of patients with pancreatic ductal adenocarcinoma: A multicenter cohort study. Gastroenterology. 2022;163(5):1252–66. e2.
16. Yin C, Liufu C, Zhu T, Ye S, Jiang J, Wang M, et al. Bladder cancer in Exosomal perspective: unraveling new regulatory mechanisms. Int J Nanomed. 2024;19:3677–95.
17. Wang J, Ma P, Kim DH, Liu BF, Demirci U. Towards Microfluidic-Based exosome isolation and detection for tumor therapy. Nano Today. 2021;37.
18. Wu Y, Wang Y, Lu Y, Luo X, Huang Y, Xie T et al. Microfluidic technology for the isolation and analysis of exosomes. Micromachines (Basel). 2022;13(10).
19. Jakobsen KR, Paulsen BS, Bæk R, Varming K, Sorensen BS, Jørgensen MM. Exosomal proteins as potential diagnostic markers in advanced non-small cell lung carcinoma. J Extracell Vesicles. 2015;4:26659.
20. Qian Q, Wei Y, Xu Y, Zheng M, Wang C, Zhang S, et al. Microfluidic magnetic detection system combined with a DNA framework-mediated immune-sandwich assay for rapid and sensitive detection of tumor-derived exosomes. Microsyst Nanoeng. 2023;9:139.
21. Yoshioka Y, Kosaka N, Konishi Y, Ohta H, Okamoto H, Sonoda H, et al. Ultra-sensitive liquid biopsy of Circulating extracellular vesicles using exoscreen. Nat Commun. 2014;5:3591.
22. Xu H, Liao C, Zuo P, Liu Z, Ye BC. Magnetic-Based microfluidic device for On-Chip isolation and detection of Tumor-Derived exosomes. Anal Chem. 2018;90(22):13451–8.
23. Trinidad CV, Pathak HB, Cheng S, Tzeng SC, Madan R, Sardiu ME, et al. Lineage specific extracellular vesicle-associated protein biomarkers for the early detection of high grade serous ovarian cancer. Sci Rep. 2023;13(1):18341.
24. Rhee HW, Zou P, Udeshi ND, Martell JD, Mootha VK, Carr SA, et al. Proteomic mapping of mitochondria in living cells via spatially restricted enzymatic tagging. Science. 2013;339(6125):1328–31.
25. Xie B, Liang X, Yue W, Ma J, Li X, Zhang N, et al. Targeting cytokinesis Bridge proteins to kill high-CIN type tumors. Fundamental Res. 2021;1(6):752–66.
26. Lin J, Chen X, Huang P. Graphene-based nanomaterials for bioimaging. Adv Drug Deliv Rev. 2016;105(Pt B):242–54.
27. Mathieu M, Nevo N, Jouve M, Valenzuela JI, Maurin M, Verweij FJ, et al. Specificities of exosome versus small ectosome secretion revealed by live intracellular tracking of CD63 and CD9. Nat Commun. 2021;12(1):4389.
28. Li M, Zeringer E, Barta T, Schageman J, Cheng A, Vlassov AV. Analysis of the RNA content of the exosomes derived from blood serum and urine and its potential as biomarkers. Philos Trans R Soc Lond B Biol Sci. 2014;369(1652).
29. Zhang W, Ou X, Wu X. Proteomics profiling of plasma exosomes in epithelial ovarian cancer: A potential role in the coagulation cascade, diagnosis and prognosis. Int J Oncol. 2019;54(5):1719–33.
30. Moore RG, McMeekin DS, Brown AK, DiSilvestro P, Miller MC, Allard WJ, et al. A novel multiple marker bioassay utilizing HE4 and CA125 for the prediction of ovarian cancer in patients with a pelvic mass. Gynecol Oncol. 2009;112(1):40–6.
31. Yu W, Hurley J, Roberts D, Chakrabortty SK, Enderle D, Noerholm M, et al. Exosome-based liquid biopsies in cancer: opportunities and challenges. Ann Oncol. 2021;32(4):466–77.
32. Dorayappan KDP, Gardner ML, Hisey CL, Zingarelli RA, Smith BQ, Lightfoot MDS, et al. A microfluidic chip enables isolation of exosomes and establishment of their protein profiles and associated signaling pathways in ovarian cancer. Cancer Res. 2019;79(13):3503–13.
33. Wang C, Zhang Y, Tang W, Wang C, Han Y, Qiang L, et al. Ultrasensitive, high-throughput and multiple cancer biomarkers simultaneous detection in serum based on graphene oxide quantum Dots integrated microfluidic biosensing platform. Anal Chim Acta. 2021;1178:338791.
34. He M, Crow J, Roth M, Zeng Y, Godwin AK. Integrated immunoisolation and protein analysis of Circulating exosomes using microfluidic technology. Lab Chip. 2014;14(19):3773–80.
35. Joazeiro CAP. Mechanisms and functions of ribosome-associated protein quality control. Nat Rev Mol Cell Biol. 2019;20(6):368–83.
36. Barron CC, Bilan PJ, Tsakiridis T, Tsiani E. Facilitative glucose transporters: implications for cancer detection, prognosis and treatment. Metabolism. 2016;65(2):124–39.
37. Dochez V, Caillon H, Vaucel E, Dimet J, Winer N, Ducarme G. Biomarkers and algorithms for diagnosis of ovarian cancer: CA125, HE4, RMI and ROMA, a review. J Ovarian Res. 2019;12(1):28.
38. Wong AH-H. Pushing the boundary of cancer diagnostics through microfluidic technologies. Innov Med. 2023;1(1):100005.
39. Ma L, Guo H, Zhao Y, Liu Z, Wang C, Bu J, et al. Liquid biopsy in cancer current: status, challenges and future prospects. Signal Transduct Target Ther. 2024;9(1):336.

Publisher's note